Interaction between coarse particles in a granular flow

Umberto d'Ortona, Nathalie Fraysse, Nathalie Thomas

Interaction between coarse particles in a granular flow

Umberto D'Ortona
*Aix-Marseille Univ., CNRS, Centrale Marseille, M2P2, Marseille, France**

Nathalie Fraysse
Université Côte d'Azur, CNRS, INPHYNI, Nice, France†

Nathalie Thomas
Aix-Marseille Univ., CNRS, IUSTI, Marseille, France‡

(Dated: February 13, 2022)

The interaction between two large particles (called tracers) in a dry granular flow made of small particles is studied experimentally and numerically. Depending on the size ratio between tracers and small particles (ranging from 6 to 13) and on the flow thickness (ranging from 6 to 30 small particle diameters) three different regimes are observed. For thin flow thicknesses, tracers get close while flowing and remain in contact. For intermediate thicknesses, tracers flow at a defined distance that increases with the flow thickness, and for large thicknesses, there is an abrupt transition above which tracers move away from each other. The transitional flow thickness increases with tracer size. More surprisingly, for all tracer sizes and all flow thicknesses, tracers get aligned with the flow. These features are explained through a mechanism involving the path of the front tracer which favors tracers regrouping, and the velocity gradient of the flow which tends to repel the tracers. Both are linked through the vertical and longitudinal spacings between tracers which modulate these effects.

I. INTRODUCTION

The interaction between sedimenting particles in a fluid is a problem that has been studied for long [1–10]. Solid spheres moving in a fluid can present a very rich phenomenology like the Drafting-Kissing-Tumbling behaviour [11–13], or like peculiar patterns [14–16], or like trains of particles in channel flow [17, 18]. In the case of non-Newtonian fluids, more complex phenomena may arise, like repulsion between particles for a shear-thickening fluid, or alignment in sheared viscoelastic fluids [19].

Contrarily to the case of a liquid, in a granular material, coarse particles do not sedimentate only because of density differences. Though, large particles having the same density can segregate toward the free surface of the granular flow as expected with granular size segregation, or can sink and move at the bottom of the flow [20–22]. This last phenomenon, called reverse segregation, is due to buoyancy. As the flowing small particles have a volume fraction around 0.6, the density ratio between a large particle and the equivalent volume of the surrounding small particles having the same intrinsic density tends to 1.7 for very large particles. The transition between segregation and reverse segregation occurs for a size ratio between large d_t and small particle d around $d_t/d \simeq 4.5$ [22]. Here, to ensure reverse segregation, large particles have a size ratio between 6 and 13.

The subject of this article is to study the interaction between two large particles, called hereafter tracers, in a granular flow made of small particles both having the same intrinsic density. Several works present results with one or more static intruders in a granular flow [23].The main difference is that in this work the tracers are free to move with the flow down a rough incline. Even though the interaction between coarse particles likely occurs in debris flows or industrial processes, it has never been studied to our knowledge. For this reason, two investigation methods, experiments and Distinct Element Method (DEM) simulations, were used. The article is organized as follows, the experimental protocol and the numerical scheme are presented. Then, part III presents the physical phenomenon and a comparison between experiments and simulations. A parametric numerical study is performed in part IV where the effects of tracer size, incline slope, incline roughness and flow thickness are considered. A mechanism is proposed in part V and the article ends with conclusions.

II. METHODS

A. Experimental protocol

Experiments have been conducted on a 80 cm long and 10 cm wide incline (Fig. 1). The incline is made rough either by covering the board with a grade P120 sandpaper or by gluing a mono-layer of 250 μm glass particles on a transparent plate, which generates a translucent plane. Both methods gives equivalent results, however, by illuminating the incline from bellow, the latter makes it possible to follow the tracers, which are colored in bulk, when the granular flow is thick and the tracers are fully embedded in the flow. The slope of the incline is equal to 24°. Flowing particles are glass beads (ρ =2500 kg m^{-3})

* umberto.dortona@cnrs.fr
† nathalie.fraysse@univ-nice.fr
‡ nathalie.thomas@univ-amu.fr

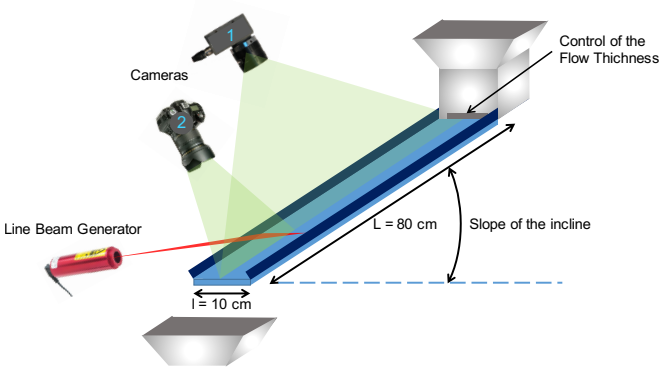

FIG. 1. Sketch of the experimental set up.

that have been sieved between 300 μm and 400 μm, with a size distribution centered on 350 μm. Tracers are glass beads (ρ =2580 kg m^{-3}) with diameters ranging from $d_t = 2.0$ mm to 4.0 mm leading to size ratio d_t/d ranging from about 6 to 11. A feeding container of an approximate volume of two liters is placed at the top of the incline. The flow rate from the hopper is controlled by the size of the container gate. Its width is kept constant and its height can be varied to obtain different thicknesses of the flow. After the opening of the gate, when a steady uniform flow of small glass beads has established over the entire channel, tracers are gently dropped on the flow about 10 cm below the upper bound of the channel as the flow thickness might not be constant above this zone. We select tracers that start close enough each other to interact. The tracers reach their stationary height inside the granular flow within a few centimeters and are driven downwards. A high-resolution video camera with a wide-angle lens, placed above the channel, images its entire length while a digital still camera, also placed above the channel, zooms in on its lower part. The positions of the tracers are obtained from videos recorded at 30 fps typically as well as from photos captured in burst mode. The thickness of the granular flow is measured from the shift of the shadow of a thin string or from the deflection of a laser sheet. Flow thickness from 2.2 mm to 2.9 mm have been studied. Ambient humidity is kept around 50%RH.

B. Numerical model

The numerical method used is the distinct element method (DEM). A linear-spring and viscous damper force model [24, 25] is used to calculate the normal force between contacting particles: $\mathbf{F}^n_{ij} = [k_n\,\delta - 2\gamma_n m_{\rm eff}(\mathbf{V}_{ij}\cdot\hat{\mathbf{r}}_{ij})]\hat{\mathbf{r}}_{ij}$ where δ and $\mathbf{V}_{ij} = \mathbf{V}_i - \mathbf{V}_j$ are the particle overlap and the relative velocity of contacting particles, respectively, $\hat{\mathbf{r}}_{ij}$ is the unit vector in the direction between two particles i and j, $m_{\rm eff} = m_i m_j/(m_i + m_j)$ is the reduced mass of the two particles, $k_n = m_{\rm eff}[(\frac{\pi}{\Delta t})^2 + \gamma_n^2]$ is the normal stiffness and $\gamma_n = \ln e\,/\Delta t$ is the normal damping with Δt the collision time and e the restitution coefficient.

A standard tangential force with elasticity is implemented: $\mathbf{F}^t_{ij} = -\min(|\mu\mathbf{F}^n_{ij}|, |k_s\zeta|)\mathrm{sign}(\mathbf{V}^s_{ij})$ where $\mathbf{V}^s_{ij}$ is the relative tangential velocity of the two particles, k_s is the tangential stiffness, and $\zeta(t) = \int_{t_0}^{t}\mathbf{V}^s_{ij}(t')\,\mathrm{d}t'$ is the net tangential displacement after contact is first established at time $t = t_0$. The gravitational acceleration is $g = 9.81\,\mathrm{m\,s^{-2}}$. The particle properties correspond to those of cellulose acetate: density $\rho = 1308\,\mathrm{kg\,m^{-3}}$, restitution coefficient $e = 0.87$ and friction coefficient $\mu = 0.7$ [24, 27–29]. To prevent the formation of a close-packed structure, the small particles have a uniform size distribution ranging from $0.95d$ to $1.05d$, with $d = 6$mm the small particle diameter. The large particle diameter (tracer) is d_t. The collision time is Δt =10^{-4} seconds, consistent with previous simulations [29–31] and sufficient for modeling hard spheres [32, 34, 35]. These parameters correspond to a stiffness coefficient $k_n = 7.32\,10^4$ N m^{-1} [24] and a damping coefficient $\gamma_n = 0.206$ kg s^{-1}. The integration time step is $\Delta t/50 = 2\,10^{-6}$ seconds to meet the requirement of numerical stability [32].

The rough inclined plane is modeled as a monolayer of small bonded particles of the same size. In one situation, the roughness of the incline is varied by using for the incline different particles d_i in the range $d_i = 0.9\,d$ to $1.5\,d$ where d is the diameter of the small flowing beads. Small beads are placed randomly in the simulation domain, along with two large particles that are placed in the domain at $0.75d_t$ above the bottom, aligned or not, close or away depending on the desired study. During 0.3 second gravity is set perpendicular to the plane, and particles fall on the sticky plane. All small beads touching the bottom of the domain ($z = 0$) stop moving and form the rough bottom of the inclined plane. The other beads will constitute the flowing granular material. With this procedure, rough inclined planes whose compacity is around 0.57 are obtained. After 0.3 second, gravity is tilted to the chosen slope (usually 24° except where otherwise stated), and the flow starts. Rough bottom particles are assumed to have an infinite mass for calculation of the collision force between flowing and fixed particles. The velocity-Verlet algorithm is used to update the position, orientation, and linear and angular momentum of each particle. Periodic boundary conditions are applied in the flowing direction x and in the transverse direction y of the simulation domain. The size of the domain is usually $L_x = 80d$ and $L_y = 40d$ in the x and y directions, but in some cases, the size is increased up to $200d \times 120d$. The position and velocity of all particles, including the tracers, are stored every 0.1 s for post-processing purpose. In part V, virtual springs are added in order to maintain tracers at a define distance (horizontal spring) or added to decrease their height difference (vertical spring).

III. RESULTS

A. Tracer interactions

The trajectory of two large tracers in a dry granular flow down a rough inclined plane is studied. Tracers and small particles have the same intrinsic density. Their size ratio is set to $d_t/d = 10$ in this first part. With such a size ratio, large tracers stabilize near the bottom of the granular flow in a reverse segregated position [20, 22]. First, three flow thicknesses have been chosen ($H = 7\,d$, $15\,d$ and $18\,d$), the slope of the rough incline is 24° and particles flow in the x-direction. The two tracers alignment is initially ($t = 0$ s) at 45° of the flow direction, and the tracer centers are at a distance equal to 2 d_t (left column of Fig. 2). For the thick flow cases, as large tracers are

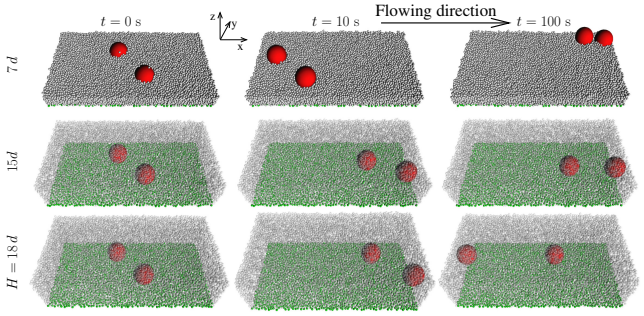

FIG. 2. Three successive positions of 2 tracers ($d_t/d = 10$) in a granular flow with three different thicknesses: $H = 7\,d$, $15\,d$ and $18\,d$. Particles of the rough incline are green. For the thick flows, small flowing particles are drown partly transparent. The simulation domain is 40 $d \times 80\,d$ and the slope is 24°. See video 1 to 3 in Supplemental Material [33]

completely embedded in the granular flow, small particles are drown partly transparent. For the thin flow, tracers are large enough to emerge from the flow and are visible at the surface. The tracers are not in contact with the rough incline, but spontaneously flows with about 3 small particles above it. This equilibrium position results from a reverse segregation because tracers are denser than the bulk around them and the difficulty to penetrate the last small particle layers near the bottom. Chain forces are efficient enough when close to the bottom to support a large tracer. Nevertheless a higher density for the tracer, or a longer break down of these chains in the tracer path, could lead to a deeper tracer position.

For the thin flow case ($H = 7\,d$), the tracers align in the flowing direction and eventually get in contact. Tracers attract each other. For the two thick flow cases, the tracers also align but move away from each other, with a distance depending on the flow thickness H. For $H = 15\,d$, tracers locate at a distance (measured from center to center) around $\Delta x = 20\,d$ For $H = 18\,d$ the distance is $\Delta x = 35\,d$, which is not far from the maximal distance ($\Delta x = 40\,d$) since the simulation domain length is $L = 80\,d$. For the thickest flow, tracers repel each other.

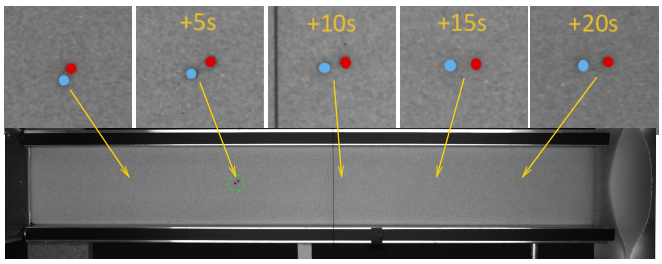

FIG. 3. Experimental system with a granular flow made of $d \simeq 340$ μm particles and two $d_t = 2$ mm tracers. The flow thickness is $H = 2.2$ mm$= 6.5d$. The lower picture shows the complete plane and one location of the tracers surrounded by a green dashed circle. The five upper sub-images show the time evolution of the relative location between tracers, and their corresponding locations on the plane. Red and blue circles are drawn on tracers, with the same diameter.

Figure 3 shows the equivalent experiment with a flowing thicknesses $H = 2.2$ mm i.e. $H = 6.5\,d$ when measured in small beads diameter $d \simeq 340\,\mu$m. The tracer size $d_t = 2$ mm corresponds to a size ratio $d_t/d = 6$, the slope incline is equal to 24° and the flow moves rightward. The five upper sub-images show the time evolution of the tracer positions. To facilitate the visualisation, their locations are highlighted by two circles of the same diameter, the red circle shows the front tracer. Like in simulations the two tracers get aligned with the flowing direction. Tracers that are initially in contact move away while flowing and eventually locate at a distance $\Delta x \simeq 2.5\,d_t = 15\,d$ from center to center.

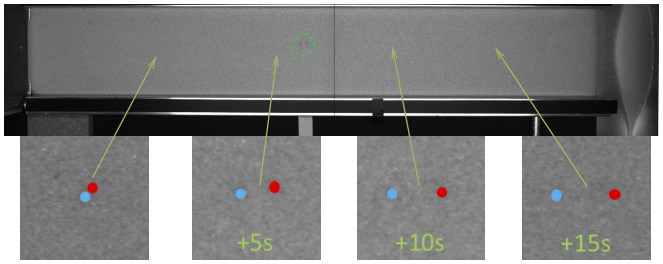

FIG. 4. Experimental system with a granular flow made of $d \simeq 340$ μm particles and two $d_t = 2$ mm tracers (positions surrounded by the green dashed circle in the flow). The flow thickness is $H = 2.9$ mm$= 8.5d$. The four lower sub-images show the time evolution of the relative location between tracers. Red and blue circles are drawn on tracers, with the same diameter.

Figure 4 shows the case of a thicker flow $H = 2.9$ mm $= 8.5\,d$. The size of the tracers, the small beads and the slope are unchanged. Like in the thin case, tracers get aligned with the flow but the distance between tracers continuously increases until tracers reach the end of the incline with a distance $\Delta x \simeq 30\,d$. Experiments confirm that depending on the flow thickness, two tracers may be in an attractive or repulsive regime while flowing.

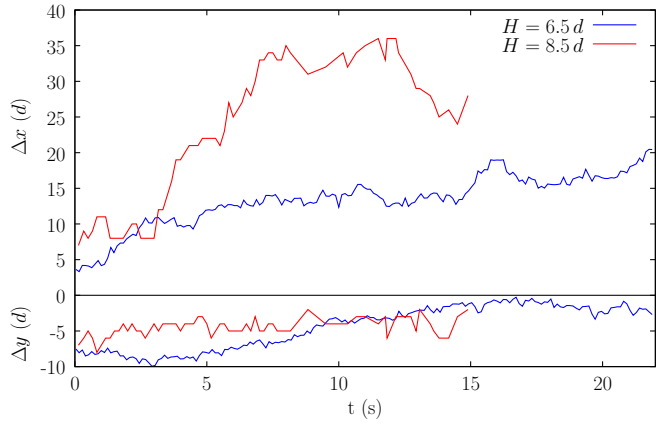

FIG. 5. Longitudinal (Δx, upper curves) and transverse (Δy, lower curves) distances between the two tracer centers ($d_t/d = 6$) measured in small bead diameter (d) for the two experimental flow thicknesses $H = 6.5\,d$ and $H = 8.5\,d$, corresponding to Figs. 3 and 4 respectively.

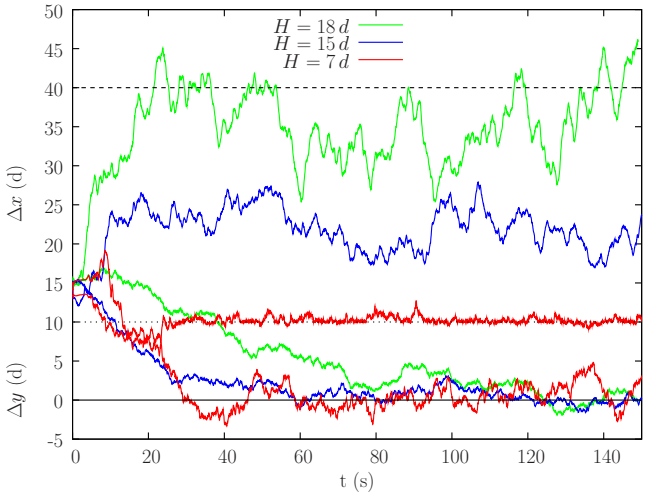

FIG. 6. Longitudinal (Δx, upper curves) and transverse (Δy, lower curves) distances between the two tracer centers ($d_t/d = 10$) measured in small bead diameter (d) for three flow thicknesses ($H = 7\,d$, $15\,d$ and $18\,d$) corresponding to Fig. 2. The transverse distances Δy converge to zero. The longitudinal distances tend to different values increasing with flow thickness. The dotted line (10 d) indicates the minimal longitudinal distance between the two tracer centers when they are perfectly aligned with the flowing direction. The dashed line (40 d) shows half of the longitudinal size of the simulation domain, i.e. the maximum distance that two aligned repelling tracers can reach.

Figure 5 shows the time evolution of the longitudinal (Δx, upper curves) and transverse (Δy, lower curves) distances between the two tracer centers ($d_t/d = 6$) for the two experimental flow thicknesses. For the thin flow ($H = 6.5\,d$ blue curves), the transverse distance Δy decreases and tends to zero, tracers get aligned. The longitudinal distance Δx, rapidly growths to $10\,d$, and then reaches some kind of plateau around $15\,d$ with a slight increase suggesting that the flow thickness is not constant. The 5 last seconds of the experiments are not considered since tracers accelerate just before falling from the incline. For the thick flow ($H = 8.5\,d$ red curves), the transverse distance also decreases, more slowly than the thin case, and does not reach zero before the end of the incline. The longitudinal distance rapidly reaches a value around $\Delta x = 30d$ and fluctuates around it. The curves for the thick flow end more rapidly than for the thin case since for a thick flow, the flowing velocity is higher.

Figure 6 shows equivalent curves for the numerical simulations with three flow thicknesses. After a transition period that depends on the flow thickness, a stationary regime is reached. The transverse distance (Δy) converges toward zero independently of the flow thickness. Like in experiments, Δy rapidly reaches zero for a thin flow, and more slowly for a thicker flow. The longitudinal distance (Δx) also converges, but presents various behaviors. For thin flows ($H = 7\,d$), the distance tends nearly to d_t (black dotted line) showing that tracers are almost in contact. For $H = 15\,d$, the longitudinal distance fluctuates around $\Delta x = 20\,d$. For the thickest flow ($H = 18\,d$), the longitudinal distance reaches almost $\Delta y = 40\,d$ which corresponds to half of the simulation domain length. The distance between two repelling tracers can not increase any further since they interact by both sides of the simulation domain because of the periodic boundary conditions.

Figure 7 plots the mean longitudinal $\langle \Delta x \rangle$ and transverse distances $\langle \Delta y \rangle$ between tracer centers with increasing flow thicknesses in the range $H = 6d, \ldots, 25d$. The error bars indicate the standard deviation of the distances. The first 50 s of each simulation are discarded to ensure that convergence is reached. Two domain sizes have been considered to understand the effect of periodic boundary conditions. For all flow thicknesses, the transverse distance (Δy) is close to zero confirming that tracers tend to align with the flow direction. The longitudinal distance (Δx) shows a transition around $H = 17\,d$. Below that thickness, tracers locate at a define distance that decreases with decreasing flow thicknesses. This decrease is limited by the size of the tracers. Indeed, Δx tends to one tracer diameter, here $d_t = 10d$ and tracers are in contact. Standard deviations are very small, indicating that the attraction between tracers is strong enough not to be sensible to the fluctuations inherent to a granular flow. Contrarily, for thick flows the longitudinal distance reaches the maximal distance $\Delta x = 40\,d$ and standard deviations are large. In the repulsive regime longitudinal distances strongly fluctuate.

To highlight the effect of the simulation domain size, this one has been increased to $160d \times 40d$ (blue triangles), but only for a few cases since simulations became numerically costly. For thin flows, the tracer longitudinal distances remain very close to those obtained for a small box. For flow thicknesses larger then $H = 17\,d$, the two tracers locate at the maximal possible distance, which is

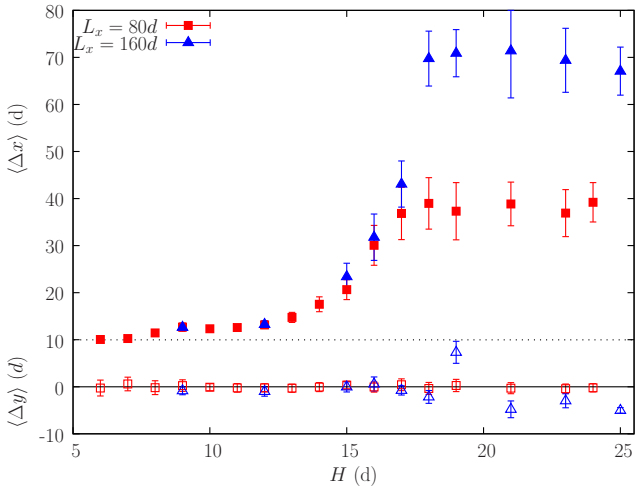

FIG. 7. Mean longitudinal $\langle \Delta x \rangle$ (filled symbols) and transverse $\langle \Delta y \rangle$ (empty symbols) distances between the two tracer centers measured in particle diameter (d) for increasing flow thicknesses H. The dotted line indicates a tracer diameter $d_t = 10d$, i.e. the minimal longitudinal distance between two aligned tracers. The simulation domain size is 80d×40d (red squares) or 160d×40d (blue triangles).

now $80\,d$. It is also interesting to note that, with the long simulation domain $L_x = 160d$, when tracers are in the repulsive regime $H \geq 18d$, they align with the flow in a less efficient way. The transverse distance reaches value as large as $\Delta y \simeq 7d$.

Two regimes can be defined, an attracting regime where tracers locate at a defined distance, and a repulsive regime. The transition between these two regimes is obtained for a threshold flow thickness H^*.

IV. PARAMETRIC STUDY

To gain a better understanding on the attractive-repulsive transition, the flow thickness, the tracer size and the slope of the incline are varied. The longitudinal and the transverse distances are measured, and also the vertical location of the tracers within the granular flow.

A. Tracer size

Three new size ratios are studied, $d_t/d = 6$, 8 and 12. Below a size ratio of 6, tracers are no more at the bottom of the flow, and undergo a classical surface segregation. For larger size ratios, the transition occurs for very large flow thicknesses and the computational cost strongly increases.

Figure 8 shows the transverse and longitudinal distances for the three tracer sizes and flow thicknesses ranging from $H = 6$ to $29\,d$. For all tracer sizes, transverse and longitudinal distances evolve in an analogous way with the flow thickness, but with some differences. The

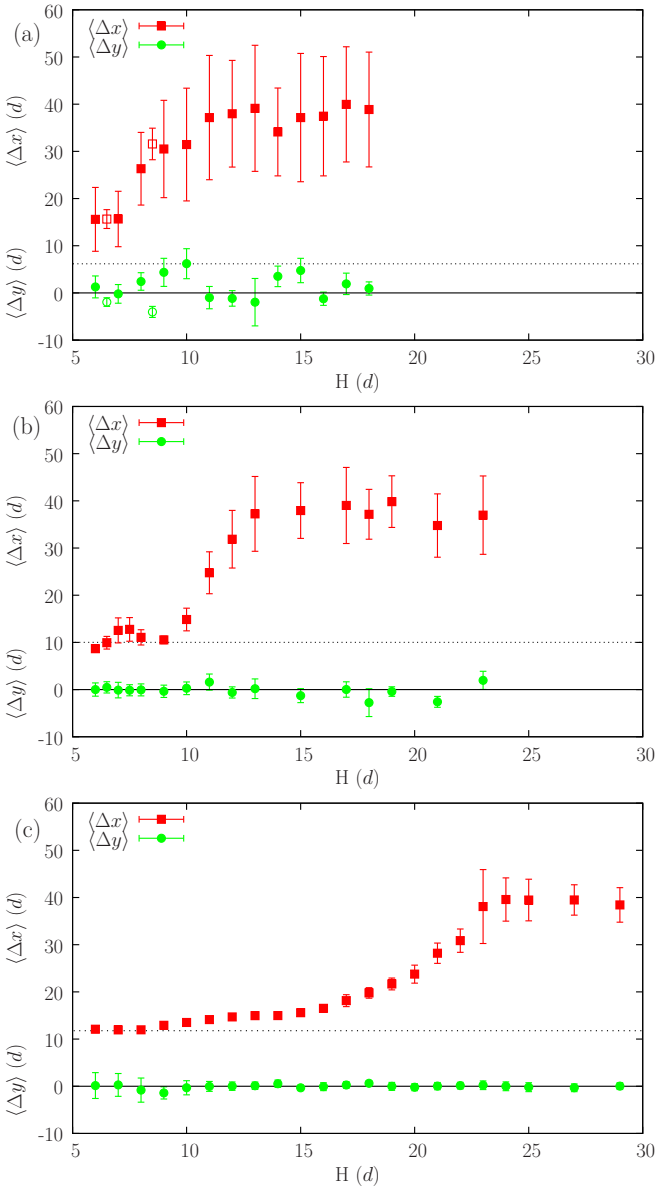

FIG. 8. Mean longitudinal $\langle \Delta x \rangle$ and transverse $\langle \Delta y \rangle$ distances between two tracers for increasing flow thicknesses. The size ratio between tracers and small particles is (a) $d_t/d = 6$, (b) $d_t/d = 8$ and (c) $d_t/d = 12$. The flow thickness range, different for each size ratio, is from $H = 6\,d$ to $29\,d$. The dotted lines indicate a tracer diameter. Both axes are kept identical to facilitate comparison. In the case $d_t/d = 6$, the empty symbols are obtained from the experiments.

transition between attractive and repulsive regimes depends on the tracer size. It occurs for flow thickness around $H^* = 11d$, $13d$, $18d$ and $22d$ for tracers of diameters $d_t = 6d$, $8d$, $10d$ and $12d$ respectively.

For the size ratio $d_t/d = 6$, all longitudinal distances have a large standard deviation, even for low flow thicknesses (Fig. 8(a)). The lower limit of the attractive regime, where tracers are in contact, can not be reached since for such low thicknesses, the flow stops. For H large

enough so that the flow occurs, the attraction between tracers is not efficient enough and tracers are never in contact. It is interesting to note that the longitudinal distances obtained in simulations, $\Delta x \simeq 16\,d$ for $H = 6\,d$ and $\Delta x \simeq 30\,d$ for $H = 9\,d$ are in a good agreement with experiments (see Fig. 5). Tracers with size ratios $d_t/d = 8$ and 12 (Fig. 8(b-c)) present similar behavior compared to the case $d_t/d = 10$. For low flow thicknesses, the tracers are attractive and locate at a define distance that depends on the flow thickness. For the lower flow thicknesses, the longitudinal distance is close to one tracer diameter and tracers are in contact. In the attractive regime standard deviations are small. For thick flows, tracers repel each other, the longitudinal distance is close to $\langle \Delta x \rangle \simeq 40\,d$ and fluctuations are large. Similar attractive and repulsive regimes are found, but the value of the transition thickness H^* depends on the tracer size.

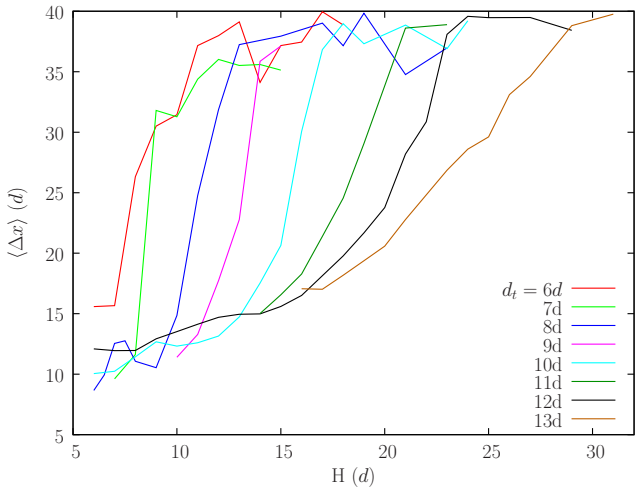

FIG. 9. Mean longitudinal distance $\langle \Delta x \rangle$ versus flow thicknesses for tracer sizes ranging from $d_t/d = 6$ to 13.

Figure 9 regroups the longitudinal distance $\langle \Delta x \rangle$ for all studied cases versus flow thickness H. Intermediate size ratios $d_t/d = 7$, 9, 11 and 13 have been added near the attractive-repulsive transition. All tracers present a transition between an attracting and a repulsive regime, but the transition is smoother for larger tracer size. For example, for $d_t/d = 8$ a flow thickness variation from $H = 9\,d$ to $H = 13\,d$ is enough to switch from tracers in contact to the repulsive regime, while for $d_t/d = 12$, a flow thickness increase from $H = 15\,d$ to $H = 23\,d$ is necessary. The overall curve organisation of Fig. 9 suggests that plotting $\langle \Delta y \rangle$ vs H/d_t might collapse the curves, but this is not the case. A better collapse is obtained with $H/d_t^{1.5}$, but we see no theoretical reason for such a choice.

This graph could be used to quantify the transition flow thickness H^* for each tracer diameter d_t. But we will see that using the vertical location of the tracers in the flow gives a more accurate criterion.

B. Tracer depth

The vertical location of the two tracers ($d_t = 10d$) for increasing flow thicknesses is now considered (Fig. 10). Let us note that compared to previous graphs, the vertical axis is strongly stretched. Several facts are noticeable.

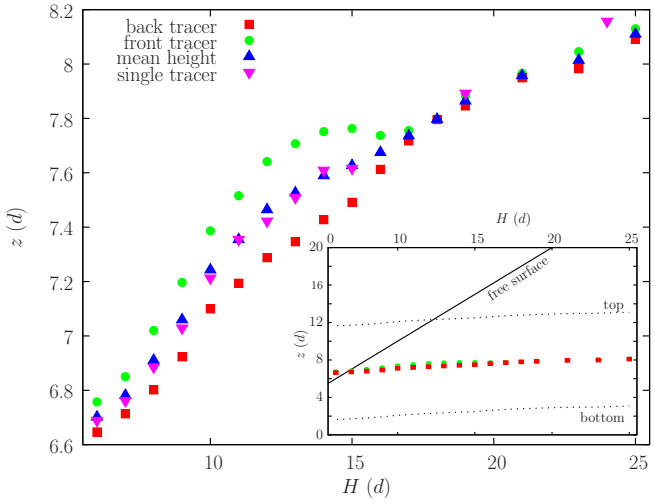

FIG. 10. Mean vertical position of the front (green circles) and back (red squares) tracers versus flow thickness H in small bead diameter d. For comparison, the center of mass of the tracers (blue triangle) and the vertical position of a single tracer in a similar flow (purple reverted triangle) are also presented. In the inset, the vertical locations of the front tracer summit and bottom (dotted lines) and of the free surface (solid line) have been added. $z = 0$ corresponds to the summit of the rough incline glued particles.

The front tracer (green circles) is upper in the flow than the back tracer (red squares), and that happens below the flow thickness $H = 18\ d$ which corresponds to the repulsive/attractive transition (see Fig. 7). For thicker flows, i.e. when tracers are in the repulsive regime and far away from each other, both tracer heights are identical. Figure 10 also reports the center of mass of the two tracers (blue triangles) and the vertical location of a single tracer in simulations of equal flow thicknesses (purple reverted triangles). In the repulsive regime, when tracers are far, their vertical locations are approximatively equal to that of one single tracer. More interestingly, in the attractive regime, the location of the center of mass of the two tracers also falls very close to that of a single tracer. The inset of Fig. 10 presents the summit and bottom of the front tracer (dotted line) and the location of the free surface (solid line). This helps to notice that in all cases, the height difference between tracers $\langle \Delta z \rangle$ is extremely small, less than half of a small particle diameter. The bottom dotted line also shows that tracers do not touch the particles of the rough incline whose summit is at $z = 0$, but two to three small particles are flowing in between. Considering the height difference between tracers $\langle \Delta z \rangle$, it increases when the flow thick-

ness decreases from $H = 18d$ down to $H = 13d$ (see also Fig. 11) which is an expected behavior since closer are the tracers, stronger is the interaction. But for thicknesses ranging from $H = 13d$ down to $H = 6d$ the height difference decreases. When looking at the free surface location (inset of Fig. 10), we see that tracers start to emerge for a flow thickness $H \simeq 13d$. While decreasing the flow thickness, the interaction between tracers that lifts the front tracer is counterbalanced by an extra buoyancy due to the emerging part of the tracer.

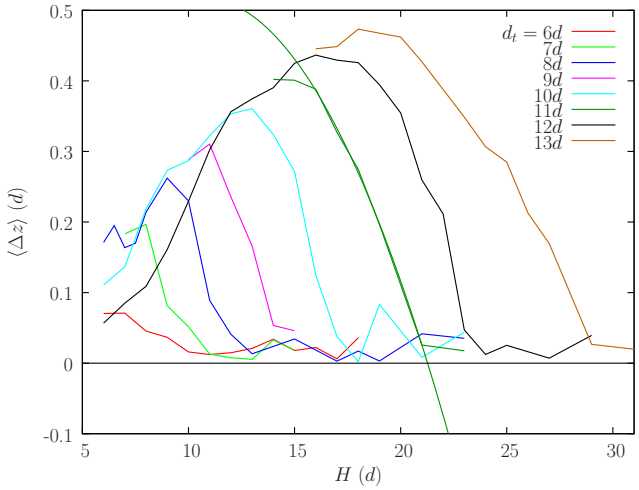

FIG. 11. Tracer height difference (Δz) versus flow thickness H in small bead diameter (d) for tracer size ranging from $d_t/d = 6$ to 13. For the case $d_t/d = 11$ a second order polynomial fitted on the descending part of the graph is showed. The intersection of this fit with the horizontal axis is used to define the transition thickness H^*

Figure 11 reports all tracer height differences with the flow thickness for tracer sizes ranging from $d_t = 6d$ to $13d$. In all cases, an increase of $\langle \Delta z \rangle$ with decreasing flow thicknesses is followed by a decrease when tracers are emerging. As expected, the maximum of the curves shifts towards low flow thicknesses for decreasing tracer sizes. For the case $d_t = 6d$, the decrease for low flow thicknesses is not obtained since in this case, no flow occurs. To obtain the flow thickness associated to the attractive/repulsive transition H^*, a second order polynomial is fitted on the right descending part of each graph. A typical example ($d_t/d = 11$) has been drawn. We define the transition thickness H^* at the intersection of the fit and the horizontal axes $\langle \Delta z \rangle = 0$, as an example $H^* = 21.3\,d$ for $d_t/d = 11$.

The evolution of the tracer height difference allows to define a transition flow thickness H^* (Fig. 12). On the same graph, the vertical location of the tracer summit for a flow of thickness H^* is reported. This vertical locations have been obtained by interpolation since no flow with the exact flow thickness H^* have been simulated. As the tracer vertical location varies very weakly with the flow thickness (see inset of Fig. 10), the interpolation gives accurate results. Other criteria have been considered to

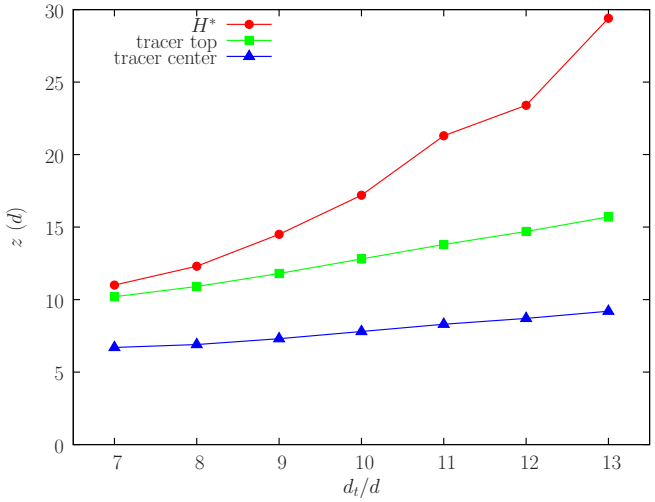

FIG. 12. Transition flow thickness H^* versus tracer size ratio d_t/d (red dot). The transition is based on the tracer height difference. Vertical location of the tracer summit (green square) and tracer center for a flow of thickness H^*.

define the transition thickness, like for example the intersection with $\Delta z = 0.5d$ in Fig. 11, and in all cases, Fig. 12 is almost identical and the conclusions are unchanged. Comparing H^* and the summit of the tracer shows that the attractive/repulsive transition does not occur when the tracer emerge from the flow. Both tracers, that have the same height at the transition, are fully embedded for a flow thickness H^*. Furthermore, the number of small flowing particles above the tracer at the transition is not constant with the size ratio d_t/d, but strongly increases.

C. Slope of the incline

The slope of the incline is now studied. The incline angle θ is varied from 22° to 25.5° for four typical cases: an attractive case ($d_t/d = 10$, $H = 11d$) where tracers are almost in contact $\langle \Delta x \rangle \simeq d_t$, a repulsive case ($d_t/d = 8$, $H = 15d$) where tracers locate at their maximal distance $\langle \Delta x \rangle \simeq 40d$, and two intermediate situations ($d_t/d = 10$, $H = 15d$ and $d_t/d = 8$, $H = 11d$) where tracers are in an attractive regime and locate at a defined distance not far from the attractive-repulsive transition. Up to now, all results were obtained for a incline angle of 24°. Figure 13 shows the mean longitudinal distance $\langle \Delta x \rangle$ for these four cases versus slope angle. For the attractive and repulsive cases, the slope has almost no effect on the distance between tracers. For the two intermediate cases, decreasing the slope angle favors the repulsive regime, and conversely increasing the slope favors the attractive regime. For the tracer diameter $d_t = 8d$, the transition is sharp and occurs between 23.5° and 24.5° while for the larger tracers $d_t = 10d$, the transition is more progressive and occurs between 22° and 24°. This is similar to the sharpness of the transition with H that becomes

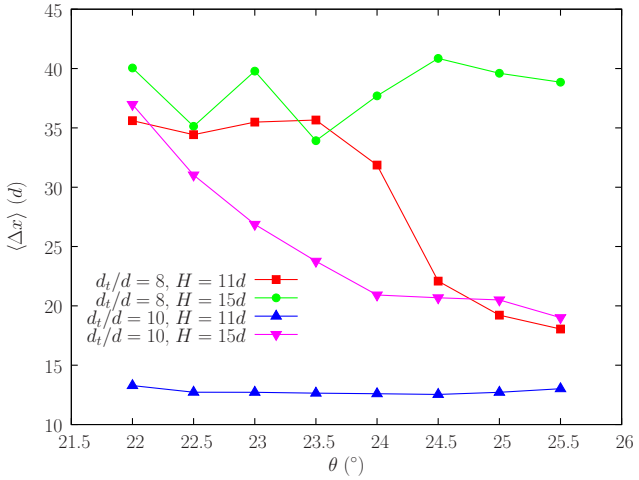

FIG. 13. Mean longitudinal distance between two tracers $\langle \Delta x \rangle$ versus slope: (red square) $d_t/d = 8$ and $H = 11d$, (green circle) $d_t/d = 8$ and $H = 15d$, (blue triangle) $d_t/d = 10$ and $H = 11d$, and (purple reversed triangle) $d_t/d = 10$ and $H = 15d$.

smoother for high d_t/d.

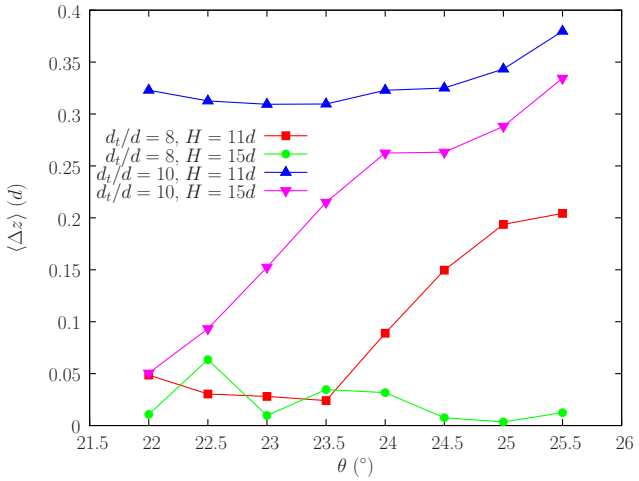

FIG. 14. Mean height difference between two tracers $\langle \Delta z \rangle$ versus slope: (red square) $d_t/d = 8$ and $H = 11d$, (green circle) $d_t/d = 8$ and $H = 15d$, (blue triangle) $d_t/d = 10$ and $H = 11d$, and (purple reversed triangle) $d_t/d = 10$ and $H = 15d$..

Figure 14 shows the height difference between tracers for increasing slope angles. It is interesting to note that Fig. 14 is close to a vertical mirror of Fig. 13. When the system moves toward the attractive regime, the distance between tracers decreases, the difference of height of the tracers increases.

The effect of angle on the attractive-repulsive transition is somehow moderate. Increasing the flow thickness from $H = 6d$ to $H = 25d$ increases the velocity by a factor 6 and allows a full transition from the lower limit of the attraction regime where tracers are in contact to the fully repulsive regime. On the other hand, increasing the slope angle from $\theta = 22$ to 25.5° increases the flow velocity by a factor 4.3 for $H = 15\,d$ and 5.6 for $H = 11\,d$ respectively, but modifies the attractive-repulsive state only when the system is already close from the transition.

D. Incline roughness

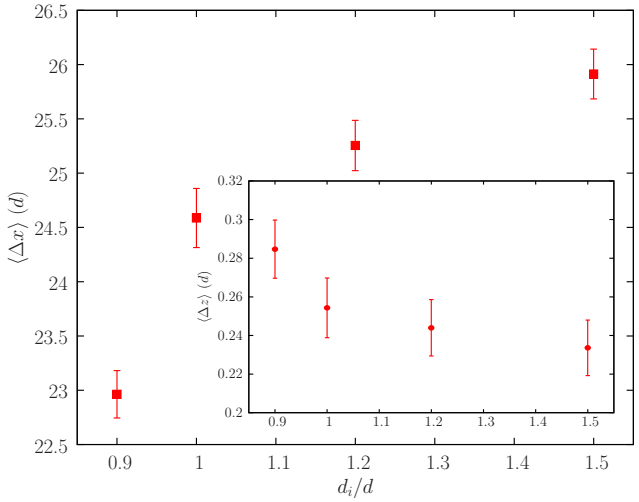

FIG. 15. Mean longitudinal distance between two tracers $\langle \Delta x \rangle$ versus incline roughness from $0.9d$ to $1.5d$. (inset) Corresponding mean height difference $\langle \Delta z \rangle$. The size ratio is $d_t/d = 10$, the flow thickness $H = 15d$ and the incline angle $\theta = 24°$. Error bars show a 95% interval of confidence of the mean value.

Another way to change the mean velocity of the flow is to change the roughness of the incline. Up to now, inclines were made with glued particles of the same size than the small flowing particles d. Here, four inclines with different roughnesses are considered with glued particles of size $d_i = 0.9\,d$, d, $1.2\,d$ and $1.5\,d$. An incline made with particles $d_i = 0.8\,d$ has been tested, but the mean velocity was extremely high indicating that a slip occurs at the base of the flowing material. Particles of size $d_i = 1.5\,d$ are the largest used since this roughness has the highest friction for a granular flow made of particle of size d [26]. Furthermore, for incline particles even larger, flowing particles fill the void between the particles of the incline and its roughness decreases. The measured mean velocity decreases while increasing the roughness, from $v_{mean} = 57$cm/s for $d_i = 0.9\,d$ to $v_{mean} = 46$cm/s for $d_i = 1.5\,d$. Even though the decrease of mean velocity is moderate, a modification of the longitudinal distance between tracers is obtained. Like by increasing the incline angle, but here, by reducing the incline roughness, when velocity increases the longitudinal distance between tracers decreases (Fig. 15). Accordingly, the difference of height between tracers $\langle \Delta z \rangle$ reduces when tracers are fur-

ther away (see inset of Fig. 15). The variations of longitudinal distance $\langle \Delta x \rangle$ and height difference $\langle \Delta z \rangle$ between tracers with incline roughness being moderate, averaging over 500 s were necessary to obtained mean value statistically significant. Nevertheless, if we compare with the effect of the variation of the incline angle, we noticed that varying the incline angle from 22° to 25.5° increases the velocity by a factor 4.3 and decreases the longitudinal distance by a factor $37/19 \simeq 1.9$. Changing the incline roughness increases the velocity by a factor 1.2 for a distance decrease by a factor $26.7/23.2 = 1.15$. In terms of variations of longitudinal distance versus flow velocity, the effect of incline roughness and incline angle are comparable.

V. A PROPOSED MECHANISM

There is a clear link between the horizontal and vertical positions of two large tracers interacting in a granular flow. Figures 13 and 14 show by varying the slope angle that when the longitudinal distance Δx decreases, the height difference Δz increases. Figure 15 leads to the same evolution by changing the incline roughness, but with weaker modifications for Δx and Δz. For both cases, the decrease of Δx and the increase of Δz go with an increase of the flowing velocity. The thickness of the flow has also an effect, but more complex. For high flow thicknesses, tracers are far away, and locate at the same height. When the flow thickness is decreased below the transition thickness H^*, the longitudinal distance Δx decreases and the height difference Δz increases (see Fig. 11). But this variation is not monotonous and when tracers start to emerge from the granular flow, their height difference decreases with the flowing thickness. Due to an "iceberg effect", the height difference induced by the decrease of Δx is counterbalanced by an extra buoyancy term that weakens the emergence of the tracers from the flow.

To get a better insight on the mechanisms acting on the pair of tracers, Fig. 16 shows the two tracers embedded in a granular flow of thickness $H = 15\,d$. Velocities and positions are in the reference frame of the front tracer (right tracer). As the relative tracer positions, Δx and Δy, fluctuate with time, two virtual springs have been added between them such that they remain in their equilibrium position [36]. The spring aligned with the flow has a length $\Delta x_0 = 20\,d$ and the transverse spring $\Delta y_0 = 0$ to force alignment. The stiffness of the springs, k_x and k_y are chosen to allow small fluctuations around the equilibrium relative positions, typically $0.5\,d$. After test and trial, a value of $k_x = k_y = k_n/20000$ is retained, where k_n is the stiffness of the normal repulsion spring between particles. Without this procedure, the fluctuations of the rear tracer position completely blurs the measured velocity vector field around it. Furthermore, we will see that the height difference Δz for tracers with two springs agrees with those of free tracers. We are

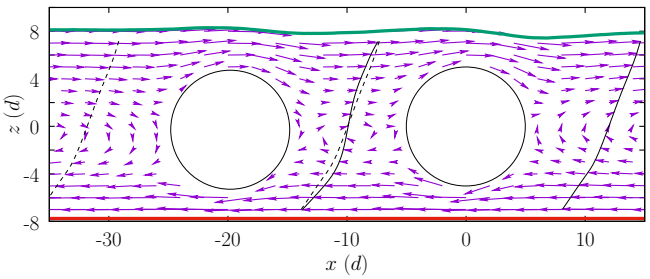

FIG. 16. Velocity map in the $z-x$ plane (vertical and aligned with the flowing direction) in the reference frame of the front tracer (right tracer). The tracer size is $d_t = 10\ d$, the flow thickness is $H = 15\,d$, and the slope angle is $\theta = 24°$. The free surface is indicated by the upper green thick line, and the bottom thick red line passes through the summit of the incline particles. The two continuous incline black lines indicate the velocity profile measured at their locations, in front of both tracers, and in between them. The two inclined dashed lines are simply copies of the front velocity profile that have been shifted horizontally to facilitate comparison.

aware of the fact that the velocity field of Fig. 16 only corresponds to the flow around two tracers being at their equilibrium positions. As soon as the tracers move out of equilibrium due to fluctuations, the velocity field is likely modified, but this will nevertheless helps to understand the involved mechanisms.

When two particles are flowing, either spheres sedimenting in a liquid or aligned cyclists, the back particle gains advantage being in the drag of the front one. Here, the picture is slightly different since tracers are in a shear flow. They move faster than the small particles flowing below them, but move slower than the upper small particles (see Fig. 16). Nevertheless, when we look at the velocity profile in between the two tracers (thick black line around $x = -10\,d$) and we compare with the velocity profile far from the tracers (thick black line around $x = 10\,d$ that has been copied as a dashed line and shifted around $x = -10\,d$ and $x = -30\,d$ to facilitate comparison), the vertical velocity gradient is decreased. The back tracers benefits from the wake of the front tracer in the lower part of the flow $-5d \lesssim z \lesssim -d$ while the front tracer benefits from the wake of the back tracer in the upper part of the flow $d \lesssim z \lesssim 5\,d$. This mechanism explains why tracers get closer. But closer are the tracers, higher is the wake effect, the velocity gradient in the region between them further decreases and tracers should finish in contact. As a consequence, another mechanism should act to repel the tracers. We already see that when the tracers are close, a height difference appears, the front tracer being higher. As tracers are embedded in a shear flow, the front tracer should go faster and tracers should move away. These two mechanisms counterbalanced each other to place tracers at an equilibrium distance. To understand the origin of the height difference, we can look at Fig. 16. The front tracer flows through bottom small particles that move slower and are

jammed between the tracer and the rough incline. The rear tracer benefit from the wake of the front tracer, the bottom small particles have a higher shear and facilitate the penetration of the rear tracer. Closer are the tracers, larger is the height difference. Figure 17 shows that there is a lower limit at this evolution. The case of a lower flow thickness is studied $H = 9\,d$ and the length of the longitudinal spring is reduced to $\Delta x_0 = 12.5\,d$. Other parameters are unchanged. As the flow thickness is decreased, tracers emerge from the flow and the height difference is reduced due to an "iceberg effect". Both the

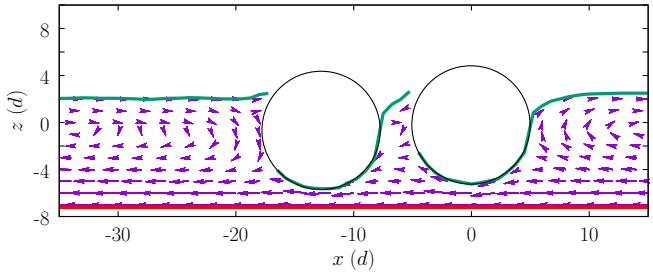

FIG. 17. Velocity map in the $z-x$ plane (vertical and aligned with the flow direction) in the reference frame of the front tracer (right tracer). The tracer size is $d_t = 10\ d$, the flow thickness is $H = 9\,d$, and the slope angle is $\theta = 24°$. The free surface is indicated by the upper green thick line, and the bottom thick red line passes through the summit of the incline particles. Tracers are not considered to obtain the free surface.

reduction of the vertical height difference and the reduction of the shear rate associated to a thin flow push the tracers to get closer.

To figure out the mechanisms involved in the convergence of tracers, another numerical experiment is performed with only one vertical virtual spring. The spring length is null $\Delta z_0 = 0$ and its stiffness is increased from $k_z = 0$ to $k_z = k_n/20000$ to reduce the tracers height difference in the flow. As there is no horizontal spring, tracers longitudinal Δx and transverse Δy distances relax to equilibrium values that depends on the height difference Δz. Tracers are initially aligned $\Delta y = 0$ and located at a longitudinal distance $\Delta x = 30\,d$ that is slightly too large for that flow thickness $H = 15d$. Let us note that for such a flowing thickness, the two tracers are fully embedded in the granular flow. Figure 18 shows the time evolution of Δx for the various vertical spring stiffness k_z. Stronger is the vertical spring that maintains the tracers at the same height, closer are the tracers. In the case of strong spring stiffness, the tracers no more stay aligned and flow side by side. This is visible since the longitudinal distance Δx becomes smaller than $\Delta x = 10\,d$ that is the minimal distance two tracers can reach when they are perfectly aligned (see dashed line). For the case $k_z = k_n/1000$, the tracers have stayed aligned up to 150 s, and then loose their alignment to flow side by side.

Figure 19 shows the vertical versus longitudinal distance between tracers. Each couple $(\Delta x,\ \Delta z)$ has been

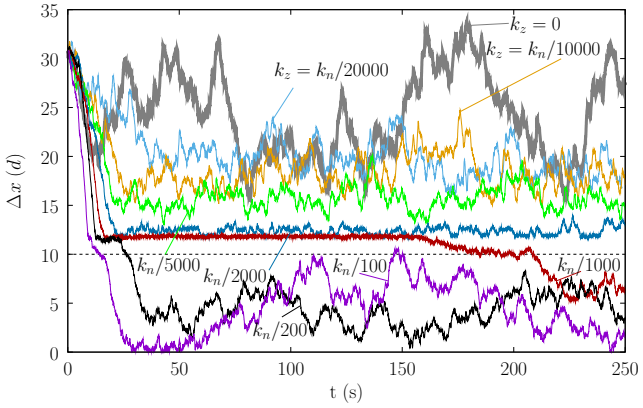

FIG. 18. Time evolution of the longitudinal distance Δx between two tracers connected by a virtual vertical spring that reduces their vertical distance Δz. The stiffness of the spring k_z varies from $k_z = 0$ (no spring) to $k_z = k_n/200$ (very strong), where k_n is the stiffness of the spring responsible of the normal force between particles. The tracer size is $d_t/d = 10$, the flow thickness is $H = 15d$ and the slope is $\theta = 24°$.

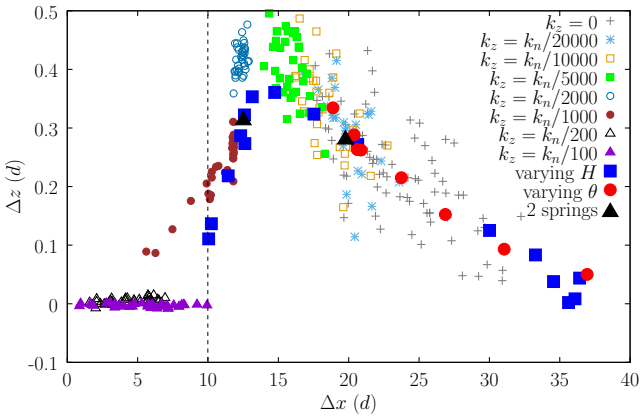

FIG. 19. Height difference Δz versus longitudinal distance Δx between tracers. The flow thickness is $H = 15\,d$ and the slope is $\theta = 24°$. The different symbols correspond to the stiffness of the vertical spring that reduces Δz. The symbol colors correspond to those of Fig. 18. The link between Δz and Δx is also extracted by varying the slope (red circles) (for $H = 15\,d$) and by varying H (blue square) for 24°, both without vertical spring. The case of tracers linked by 2 springs is added (Figs. 16 and 17) with $H = 15\,d$ and $9\,d$.

obtained by averaging for period of 5 s, the first 50 s are discarded to ensure convergence. It is interesting to note that even though there is randomness, the series corresponding to each spring stiffness are organised to follow the overall curve evolution obtained with the variation of H. This suggest that the height difference Δz rapidly adjusts to the longitudinal distance Δx while tracers are flowing. This is more clear for low Δx values corresponding to a strong tracer interaction. For larger longitudinal distances, the randomness is larger and the evolution is less visible. Superimposed with the previous

points are the vertical and horizontal distances between tracers obtained by varying the thickness of the flow H (large blue squares) for a slope of 24° and by varying the slope angle (large red dots) for a flow thickness $H = 15\,d$. The two last points (large black triangle) show the couples (Δx, Δz) obtained when two horizontal springs were used to obtained the velocity maps of Figs. 16 and 17. As these points perfectly match with the other ones, we are confident that the horizontal springs are weak enough to not perturb the tracer locations while measuring the velocity maps. Figure 19 shows that the reduction of the height difference between tracer Δz, either because the flow is thin and tracers emerge, or because a strong vertical spring is added to reduce Δz, reduces the longitudinal distance between tracers Δx.

The second limiting regime is when tracers are far away such that they no longer interact. This regime appears when the flowing thickness becomes large. As the thickness increases, the shear of the granular flow increases as well which favors the repelling mechanism. Futhermore, as tracers move away, they do not benefit of the wake of the other tracer any longer.

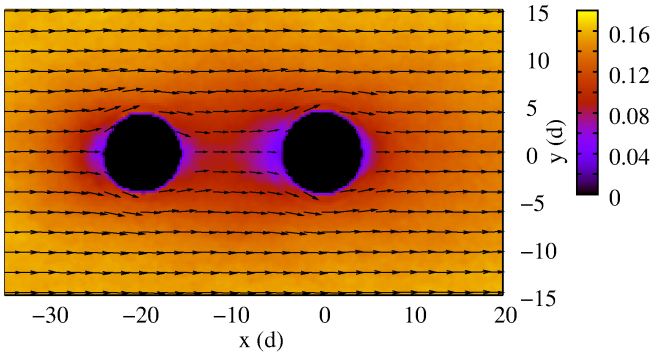

FIG. 20. Velocity map in the $x - y$ plane (parallel to flowing and transverse directions) in the reference frame of the front tracer taken at $z = 2.5d$. The color map indicates the velocity in m/s.

The last question that remains to be answered is why do tracers align within the flow? Figure 20 shows a horizontal velocity map measured at a height $d_l/4 = 2.5\,d$ above the front tracer center, half way between the center and the summit of the tracer, corresponding to $z = 2.5\,d$ in Fig. 16. As tracers are in a shear flow, the small particles being higher move faster. The darker zone between the tracers shows the wake made by the rear tracer. If the front tracer loose alignment, it will feel particles that move faster, and that will push the tracer back. The same graph can be made at $z = -2.5\,d$, half way between the tracer and the its bottom. The figure is nearly identical except that the vectors are in the opposite direction. In this case, the rear tracer is in the wake of the front tracer. In the attraction regime, tracers are close, the wake is strong and tracers are perfectly aligned. In the repelling regime, tracer are distant, they weakly fell the wake of the other tracer and the transverse distance has large fluctuations.

VI. CONCLUSION

The interaction of two large tracers in a flow down a rough incline depends on flow thickness, roughness of the incline, slope and size of the tracers. Tracers always align because tracers are embedded in a shear flow and depending on the heigh, each tracer is in the wake of the other tracer. This effect align them and also tends to get them close from each other. In addition, tracers are floating just above the bottom, at an equilibrium level inside the flow. This equilibrium results from their high density compare to the bulk density of the small particles plus the void between them, and the difficulty for a tracer to penetrate very close to the rough incline because of efficient chain forces in the first 2-3 layers of small particles. These large tracers are in a reverse segregated position. The chain forces through small particles near the bottom slow down the tracer. Nevertheless, it is possible for a tracer to get further close to the incline, either if the structure of the flow is modified, either by increasing the force (increasing tracer density for exemple) endured by the tracer to get down. When the rear tracer is in the path of the front one, the rear tracer experiences a modified structure of the flow and it gets closer to the bottom than the front tracer. In addition, the two tracers go faster than a unique tracer, and this lift the front tracer. The resulting height difference between tracers is very small, but enough to ensure that both tracers are surrounded by small particles with a slightly different velocity. The center of mass of the front tracer being upper in the velocity gradient of the flow, it tends to move faster than if it was in a lower position. The height difference between tracers in a velocity gradient tends to repel the two tracers. The resulting relative positions of the two tracers comes from the balance between the wake effect and the height difference. The interaction between two tracers implies equilibrium position of reverse segregation in accordance with their velocity and the flow structure, and velocity gradient of the flow that depends on the flow thickness, slope and roughness of the incline. This explains why the increase of flow thickness, the decrease of slope, the increase of roughness, the decrease of tracer size all tend to repel the tracers.

ACKNOWLEDGMENTS

Centre de Calcul Intensif d'Aix-Marseille University is acknowledged for granting access to its high performance computing resources.

[1] M. Smoluchowski, Bull. Acad. Sci. Cracow **1A**, 28 (1911).
[2] M. Mason and W. Weaver, Phys. Rev. **23**, 412 (1924).
[3] G. J. Kynch, Trans. Faraday Soc. **48**, 166 (1952).
[4] J. F. Richardson and W. Zaki, Trans. Inst. Chem. Eng. **32**, 35 (1954).
[5] J. Happel and H. Brenner, *Low Reynolds Number Hydrodynamics*, Prentice-Hall (1965).
[6] G. K. Batchelor, J. Fluid Mech. **52** 245 (1972).
[7] G. K. Batchelor, J. Fluid Mech. **119** 379 (1982).
[8] L. Durlofsky, J. F. Brady, and G. Bossis, J. Fluid Mech. **180**, 21 (1987).
[9] S. Kim and S. J. Karrila, *Microhydrodynamics: Principles and Selected Applications*, Butterworth-Heinemann, (2005).
[10] A. Doostmohammadi and A. M. Ardekani, Phys. Rev. E **88**, 023029 (2013).
[11] A. Fortes, D. Joseph, and T. Lundgren, J. Fluid Mech. **177**, 467 (1987).
[12] R. Sun and A. Chwang, Phys. Rev. E **76**, 046316 (2007).
[13] J. Favier, A. Revell, and A. Pinelli, J. Comp. Phys. **261**, 145 (2014)
[14] K. O. L. F. Jayaweera and B. J. Mason, Experiment. J. Fluid Mech. **20**, 121 (1963).
[15] B. Metzger , M. Nicolas and E. Guazelli, J. Fluid Mech. **580**, 283 (2007).
[16] A. El Yacoubi, S. Xu, and Z. J. Wang, J. Fluid Mech. **705**, 134 (2012)
[17] J.-P. Matas, V. Glezer, E. Guazzelli, and J. F. Morris, Phys. Fluids **16**, 4192 (2004)
[18] K. J. Humphry, P. M. Kulkarni, D. A. Weitz, J. F. Morris, and H. A. Stone, Phys. Fluids **22**, 081703 (2010)
[19] I. S. Santos de Oliveira, A. van den Noort, J. T. Padding, W. K. den Otter, and W. J. Briels, J. Chem. Phys. **135**, 104902 (2011)
[20] N. Thomas, Phys. Rev. E **62**, 961 (2000).
[21] G. Félix and N. Thomas, Phys. Rev. E **70**, 051307 (2004).
[22] N. Thomas and U. D'Ortona, Phys. Rev. E **97**, 022903 (2018).
[23] R. López de la Cruz and G. Caballero-Robledo, J. Fluid Mech. **800**, 248 (2016)
[24] J. Schäfer, S. Dippel, and D. E. Wolf, J. Phys. 1 (France) **6**, 5 (1996).
[25] P. A. Cundall and O. D. L. Starck, Géotechnique **29**, 47 (1979).
[26] C. Goujon, N. Thomas, and B. Dalloz-Dubrujeaud, Euro. Phys. J. E **11**, 147 (2003).
[27] T. G. Drake and R. L. Shreve, J. Rheol. **30**, 981 (1986).
[28] S. F. Foerster, M. Y. Louge, H. Chang, and K. Allia, Phys. Fluids **6**, 1108 (1994).
[29] Z. Zaman, U. D'Ortona, P. B. Umbanhowar, J. M. Ottino, and R. M. Lueptow, Phys. Rev. E **88**, 012208 (2013).
[30] N. Taberlet, M. Newey, P. Richard, and W. Losert, J. Stat. Mech. P07013 (2006).
[31] P. Chen, J. M. Ottino, and R. M. Lueptow, New J. Phys. **13**, 055021 (2011).
[32] G. H. Ristow, Pattern Formation in Granular Materials (Springer-Verlag, Berlin, 2000).
[33] See Supplemental Material at [href will be inserted by editor].
[34] C. S. Campbell, J. Fluid Mech. **465**, 261 (2002).
[35] L. E. Silbert, G. S. Grest, R. Brewster, and A. J. Levine, Phys. Rev. Lett. **99**, 068002 (2007).
[36] F. Guillard, Y. Forterre, and O. Pouliquen, J. Fluid Mech. **807** (2016).